Architectonics of Zinc Oxide Nanorod Coatings for Adsorption Gas Sensors

A. A. Ryabko[a,*], **S. S. Nalimova**[b], **N. V. Permyakov**[b], **A. A. Bobkov**[b], **A. I. Maksimov**[b], **V. M. Kondratev**[c,f], **K. P. Kotlyar**[c,d], **M. K. Ovezov**[b], **A. S. Komolov**[e], **E. F. Lazneva**[e], **V. A. Moshnikov**[b], and **A. N. Aleshin**[a]

[a] *Ioffe Institute, St. Petersburg, 194021 Russia*

[b] *St. Petersburg State Electrotechnical University "LETI," St. Petersburg, 197022 Russia*

[c] *St. Petersburg National Research Academic University named after Zh.I. Alferov, Russian Academy of Sciences, St. Petersburg, 194021 Russia*

[d] *Institute of Analytical Instrument Making, Russian Academy of Sciences, St. Petersburg, 190103 Russia*

[e] *St. Petersburg State University, St. Petersburg, 199034 Russia*

[f] *MIPT Center for Photonics and Two-Dimensional Materials, Dolgoprudny, 141701 Russia*

* e-mail: a.a.ryabko93@yandex.ru, sskarpova@list.ru

Received June 13, 2023; revised July 14, 2023; accepted July 31, 2023

Abstract—A method for the formation of nanostractured coatings from ZnO nanorods for use in adsorption gas sensors is presented. It has been shown that ultrasonic spray pyrolysis provides the formation of local growth centers for the formation of ZnO nanorods by the low-temperature hydrothermal synthesis. The obtained ZnO nanorods with a small diameter demonstrate a high concentration of oxygen vacancies in the near-surface region of the nanorods and a high surface concentration of hydroxyl groups. An additional method is proposed for testing seed layers by resistance using a liquid probe based on an indium-gallium melt without the need to apply top contacts. The presented technique is suitable for mass production of sensor coatings. The obtained nanostructured coatings from ZnO nanorods demonstrate a high gas analytical response.

INTRODUCTION

Adsorption resistive gas sensors based on nanostructured metal oxides are used to detect toxic and flammable gases in the surrounding atmosphere, in medical diagnostics, as a rule, they are characterized by low cost, high sensitivity and good response speed [1–5]. Currently, there are two main directions of development of adsorption gas sensors: the creation of multisensors of "electronic nose" type to determine the composition of the gas mixture, as well as the creation of adsorption sensors that work at room temperature, where optical generation of charge carriers is often used to activate gas sensitivity [6–13]. Nevertheless, such characteristics of adsorption gas sensors as high sensitivity and low cost are also key for the further development and practical application of sensors.

As a sensor material, one-dimensional nanostructures are particularly attractive, the use of which can lead to an increase of the reaction rate and recovery of the sensor due to faster transport of charge carriers than in structures that consist of particles forming many potential barriers for transport of charge carriers [14–19]. At the same time, the diameter of the nanorods should be small enough (commensurate with the value of the Debye screening depth) so that the effect of changing the cross-section of the conduction channel is significant when oxygen is adsorbed in a charged form. Zinc oxide nanorods [17–22] are widely used as one-dimensional structures for gas sensors. This is due not only to the physical properties of the material, but also to the possibility of synthesis of such structures by the low-temperature hydrothermal method. The method allows controlling the morphology of ZnO nanocrystals and hierarchical structures based on them in a wide range, and also due to the low synthesis temperature ($T < 100°C$) does not require the use of special equipment, except for the thermostat [23–28].

ZnO nanorods are applied to a substrate with electrodes by centrifugation and irrigation methods to form the sensor layer. The filamentous shape of the nanocrystals also makes it possible to synthesize the sensor layer directly on the substrate. This approach to the formation of the sensor layer ensures its adhesion to the substrate surface. Hydrothermal synthesis of nanorods on a substrate requires the presence of nucleation centers for subsequent growth of nanocrys-

tals. Seed nanocrystals which are pre-applied to the surface of the substrate are used as such centers. Seed layers for the subsequent synthesis of zinc oxide nanorods are most often formed in laboratory studies by centrifugation, which is usually accompanied by good gas sensitivity of the final nanostructured coatings [8, 29, 30]. However, the use of centrifugation in the mass production of resistive gas sensors is difficult.
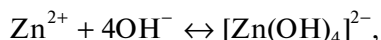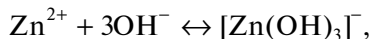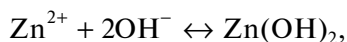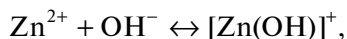
The aim of this work was to obtain nanostructured sensor layers from zinc oxide nanorods using a scalable technique based on a low-temperature hydrothermal method using seed layers obtained by ultrasonic spray pyrolysis. The technique used in this work is considered as suitable for mass production of adsorption sensor coatings based on ZnO nanorods.
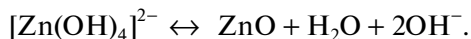
1. EXPERIMENT

Coatings made of ZnO nanorods were formed using a low-temperature hydrothermal method, in which a decrease of the operating temperature of the synthesis was provided by using sources of hydroxyl groups. In this work, hexamethylenetetramine (HMTA) was used as a source of hydroxyl groups $C_6H_{12}N_4$, capable of maintaining the pH of the medium for a long time due to the mutual impact of ongoing reactions [25]:

$$C_6H_{12}N_4 + 6H_2O \leftrightarrow 4NH_3 + 6HCHO,$$

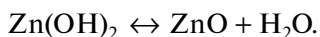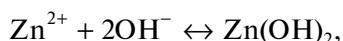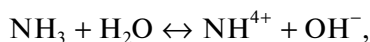$$NH_3 + H_2O \leftrightarrow NH_4^+ + OH^-$$

The rate of hydrolysis of HMTA decreases with the increase of pH and increases with the decrease of pH. Zinc nitrate (hexahydrate, $Zn(NO_3)_2 \cdot 6H_2O$) was used as a zinc source for the formation of ZnO nanorods. Zinc nitrate, when dissolved, forms zinc ions Zn^{2+}, which interact with hydroxide ions OH^- and form zinc hydroxides, which pass into zinc oxide at the operating temperature of synthesis:

$$Zn^{2+} + OH^- \leftrightarrow [Zn(OH)]^+,$$

$$Zn^{2+} + 2OH^- \leftrightarrow Zn(OH)_2,$$

$$Zn^{2+} + 3OH^- \leftrightarrow [Zn(OH)_3]^-,$$

$$Zn^{2+} + 4OH^- \leftrightarrow [Zn(OH)_4]^{2-},$$

which then condense as oxide:

$$[Zn(OH)_4]^{2-} \leftrightarrow ZnO + H_2O + 2OH^-.$$

The reactions occurring in solution can be summarized as follows:

$$NH_3 + H_2O \leftrightarrow NH^{4+} + OH^-,$$

$$Zn^{2+} + nNH_3 \leftrightarrow [Zn(NH_3)n]^{2+},$$

$$Zn^{2+} + 2OH^- \leftrightarrow Zn(OH)_2,$$

$$Zn(OH)_2 \leftrightarrow ZnO + H_2O.$$

Thus, in the process of hydrothermal synthesis, the formation of ZnO nanorods with a wurtzite structure is ensured. The concentration of zinc nitrate and HMTA was chosen equimolar (10 mmol/l), which, according to the literature, provides the highest aspect ratio of ZnO [26] nanorods. Additionally, cetyltrimethylammonium bromide (CTAB) was added to the growth solution $C_{16}H_{33}N(CH_3)_3Br$ (with a concentration of 1 mmol/l), as a surfactant substances. CTAB can additionally promote preferential growth along the [0001] direction, i.e., increase the aspect ratio of the nanorods, and also serve as an agglomeration inhibitor, forming a coating film on the ZnO [31] crystal. Low-temperature hydrothermal synthesis was carried out in a circulation thermostat (LOIP LT-208a) at a temperature of 86°C for 1 h. After synthesis, the samples were annealed in a muffle furnace in an air atmosphere at a temperature of 500°C for 5 min.

The seed layer was applied before the hydrothermal synthesis stage by ultrasonic spray pyrolysis to ceramic substrates with counter-pin NiCr/Ni/Au electrodes for obtaining a sensor coating from ZnO nanorods (Sensor Platform, Tesla Blatna). The width of the NiCr/Ni/Au electrodes on the substrate and the distance between them was approximately 25 μm. The ultrasonic spray pyrolysis was carried out using silicon substrates for optimization of the duration of application of the ZnO seed layer to study the morphology of coatings by atomic force microscopy and transparent substrates were used for determining the thickness of the ZnO seed layers. The thickness of the thickest (reference) film ZnO (~130 nm) was determined using ellipsometry (LEF-2). Effective thickness values for thin films were determined relative to the reference film by optical density spectra at a wavelength of 350 nm, since films obtained within units of minutes had a more porous or insular structure. The resistance of the obtained seed layers was also measured using a liquid probe based on eutectic indium-gallium melt (eGain) by controlled supply of a liquid probe with the formation of a contact of the same spot area. The supply of a liquid probe formed in the form of a cone and the size of the contact spot area was guided by the optical microscope. The use of a liquid eGain probe allows reducing the pressure and mechanical deformation of the studied samples [32]. Transparent conductive coatings (~10 Ω/sq) based on indium tin oxide (ITO) on glass substrates were used as the lower electrode. The ITO-coated substrates were pre-sorted to reduce the effect of resistance deviations.

Seed layers with an effective thickness of ~13.3 and 2.3 nm were used for the synthesis of sensor coatings from nanorods and subsequent measurements of gas sensitivity based on the results of studies of seed layers. The gas sensitivity of sensor coatings was measured using the developed test bench at a temperature of ~150°C and using isopropyl alcohol vapors as the analyzed reducing gas [33]. The heating temperature of the sensor coating reduced to 150°C is characterized

by safer modes for measuring the gas content at high concentrations near the explosive limit. The concentration range of isopropyl alcohol ranged from 200 to 1000 ppm. The current through the samples was recorded using a Keithley 6485 picoammeter.

The optical density spectra of the seed layers were determined using a PE-5400UF spectrophotometer. The morphology of the seed layers was studied using the Integra Terma probe nanolab (NT-MDT). The morphology of the nanostructured sensor coating made of ZnO nanorods was recorded using a Zeiss Supra 25 scanning electron microscope. The surface of the ZnO nanorods was studied using X-ray photoelectron spectroscopy (XPS). The XPS study was carried out in ultrahigh vacuum conditions (~10^{-7} Pa) using a complex photoelectron spectrometer Escalab 250Xi (Thermo Fisher Scientific Inc.) with the energy of exciting radiation Al K_α = 1486 eV. The RFES spectra were processed using the CasaXPS software version 2.3.24.

2. FINDINGS AND DISCUSSION

SEM image of the formed sensor coating of ZnO nanorods on a ceramic substrate with counter-pin electrodes is shown in Fig. 1. Darker areas in the SEM image represent the coating of nanorods formed on the interelectrode regions of a ceramic substrate, which is shown on an enlarged scale in the insert on the right. The lighter areas of the substrate represent a coating of nanorods formed on the surface of Au electrodes that, accordingly, does not participate in electrical conductivity. The gas-sensitive response is due only to the ZnO nanorods in the interelectrode region. As can be seen, the coating in the interelectrode region consists of arrays of ZnO nanorods that are in contact with each other, which is due to the topology of the surface of the ceramic substrate.

The selected concentrations of precursors and surfactant (CTAB) in an aqueous solution for low-temperature hydrothermal synthesis allow for the formation of elongated ZnO nanocrystals on the substrate surface. These nanocrystals have a diameter of only 10−20 nm, which can ensure a high gas-analytical response. However, nanorods with a diameter of more than 1 μm are also observed on the surface of the sample, which were formed in the volume of the solution, and then fixed on the surface of the sample. It should be noted that, as a rule, the ZnO nanorods formed in solution form agglomerates, while in this experiment the nanorods are formed in solution mainly in the form of separate rods, which confirms the literature data on the possible function of CTAB as an inhibitor of agglomeration. As can be seen from the SEM image, the formation of agglomerates in the form of spherical hierarchical structures from ZnO nanorods is statistically possible and may be associated with the micelle-forming function of CTAB in some areas of
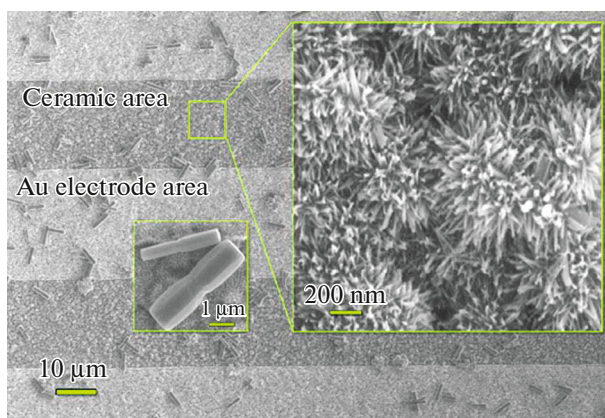

Fig. 1. SEM image of a typical sensor layer of zinc oxide nanorods obtained by sequential ultrasonic spray pyrolysis and hydrothermal method for 1 h.

the solution. Large ZnO nanorods formed in solution can perform a shunting role to the resistance of the coating of ZnO nanorods, especially when using a distance between the electrodes comparable to their length, and dramatically reduce the gas sensitivity of the sample. Therefore, it is advisable to carry out the synthesis in such a way that the seed layer on the surface of the substrate is directed downward in order to reduce the number of dropped nanorods on the surface of the sensor coating, as well as to conduct ultrasonic processing of samples for mechanical cleaning from large nanorods.

The results of X-ray photoelectron spectroscopy of the surface of the ZnO nanorods are shown in Fig. 2. The most intense peaks of the core levels of Zn2p (doublet) and O1s are observed on the survey XPS spectrum (Fig. 2a). There were also less intense peaks of photoemission from the core levels of zinc Zn2s, Zn3s, Zn3p, Zn3d and Auger electrons O KLL and ZnLMM. The spectrum shows a core level of residual carbon C1s in addition to the peaks of the core levels of the main elements such as oxygen and zinc, which is associated with the adsorption of carbon-containing compounds from the air atmosphere and, probably, incomplete desorption of carbon monoxide during the annealing of the sample. A detailed decoding of the survey spectrum was performed according to [34]. The proportion of carbon on the sample surface according to the XPS data was ~14.51% without additional treatment of the sample surface and 8.49% after treatment with an ion beam Ar$^+$ with an accelerating voltage of 500 V for 60 s. The ratio of zinc atoms to oxygen in the near-surface region of the nanorods was 1.2:1 before purification Ar$^+$ and 1.4:1 after purification. A decrease of the surface concentration of oxygen-containing and carbon-containing impurities as a result of beam treatment Ar$^+$ was observed earlier in studies of nanomaterials based on ZnO [35]. Thus, it is obvious that the
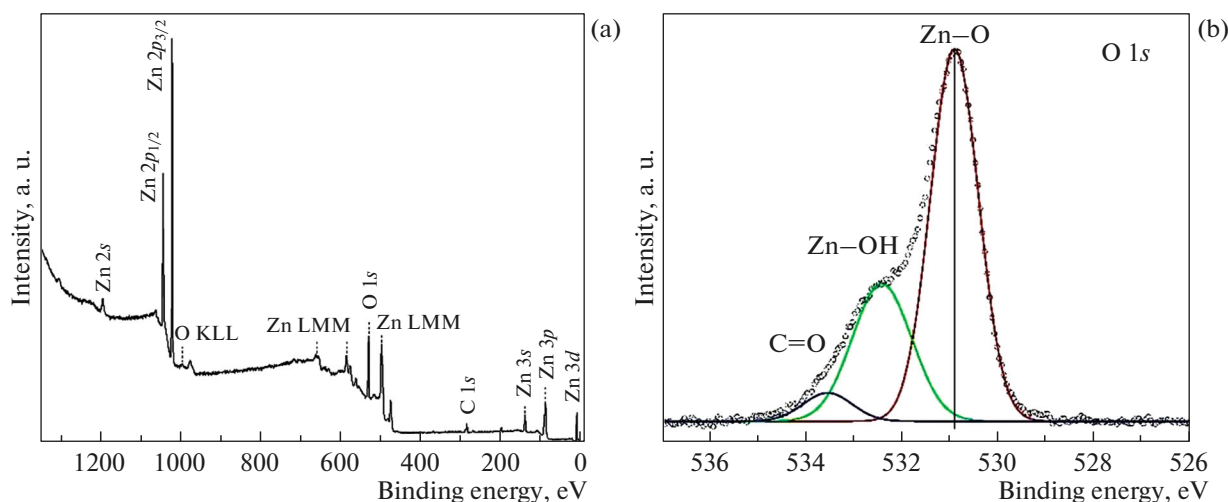
Fig. 2. XPS spectra of the surface of ZnO nanorods: (a) overview spectrum of the surface of ZnO; (b) spectrum of the core oxygen level O1*s*.

near-surface region of the ZnO nanorods contains a high concentration of oxygen vacancies.

The main oxygen peak in the zinc oxide crystal lattice (~530.9 eV) and a distinct second peak are observed in the detailed spectrum of the O1*s* core oxygen level (Fig. 2b), which, according to [36−39], bound to oxygen in adsorbed OH groups (~532.5 eV) on the surface of ZnO. Since the peak of the core carbon level is observed in the XPS spectrum, part of the O1*s* spectrum should also be due to oxygen in adsorbed compounds with carbon (~533.5 eV). Deconvolution of the O1*s* spectrum was carried out according to [36, 37].

We assume that the high concentration of oxygen vacancies and the predominance of zinc atoms in the

near-surface layer of ZnO contribute to the adsorption of OH groups. In turn, the resulting ratio of zinc and oxygen atoms is largely due to the annealing process of the samples at 500°C after synthesis. An increase of the concentration of OH groups on the surface of ZnO nanoparticles, according to the literature, leads to an increase of the efficiency of ZnO photocatalysis, and, accordingly, should contribute to an increase of the gas-analytical response [40].

The value of the thickness of the thicker film ZnO, which was determined using ellipsometry, was 130 nm. The optical density values (Fig. 3) at a wavelength of 350 nm (which corresponds to an energy less than the band gap width for zinc oxide films $E_g \approx 3.3$ eV) were compared with the value of the optical density of a thick film of known thickness to determine the effective thickness of the remaining zinc oxide layers obtained by ultrasonic spray pyrolysis with a short duration of aerosol spraying.

The results of the study of the topology of samples of seed layers by atomic force microscopy are shown in Fig. 4. As can be seen from AFM images, the seed layers of ZnO with an effective thickness of 13.3 and 19.9 nm (Figs. 4b, 4c) are ZnO crystallites with characteristic dimensions of 30−50 nm and distinct crystallite boundaries. An increase of the duration of application of the seed layer and, accordingly, the thickness in this range leads to a slight increase of crystallites without a significant change in morphology.

A significant increase of the duration of application (Fig. 4a) leads to the proliferation of crystallites, the continuity of the film is observed. The topology of the sample with an effective thickness of 2.6 nm (Fig. 4d) is a coating with a slight relief, the initial stages of the formation of individual crystallites of the film are observed. The results of measuring the resistance of the seed layer with $h_{eff} \approx 2.6$ nm, measured using the upper contact based on a liquid probe, confirm the
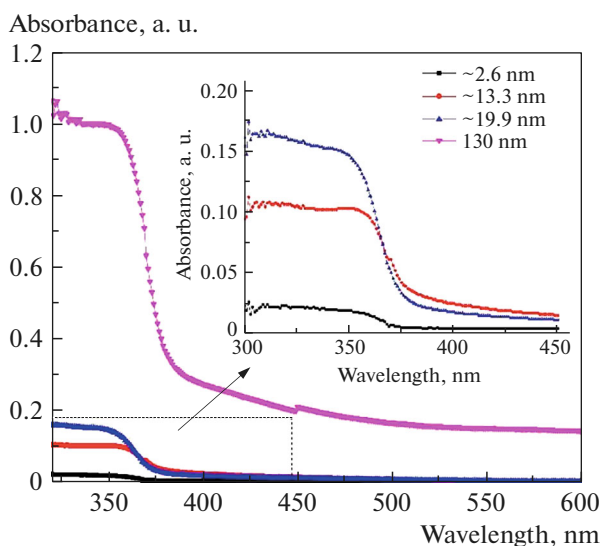

Fig. 3. Optical density of seed layers obtained by ultrasonic spray pyrolysis with varying application duration.
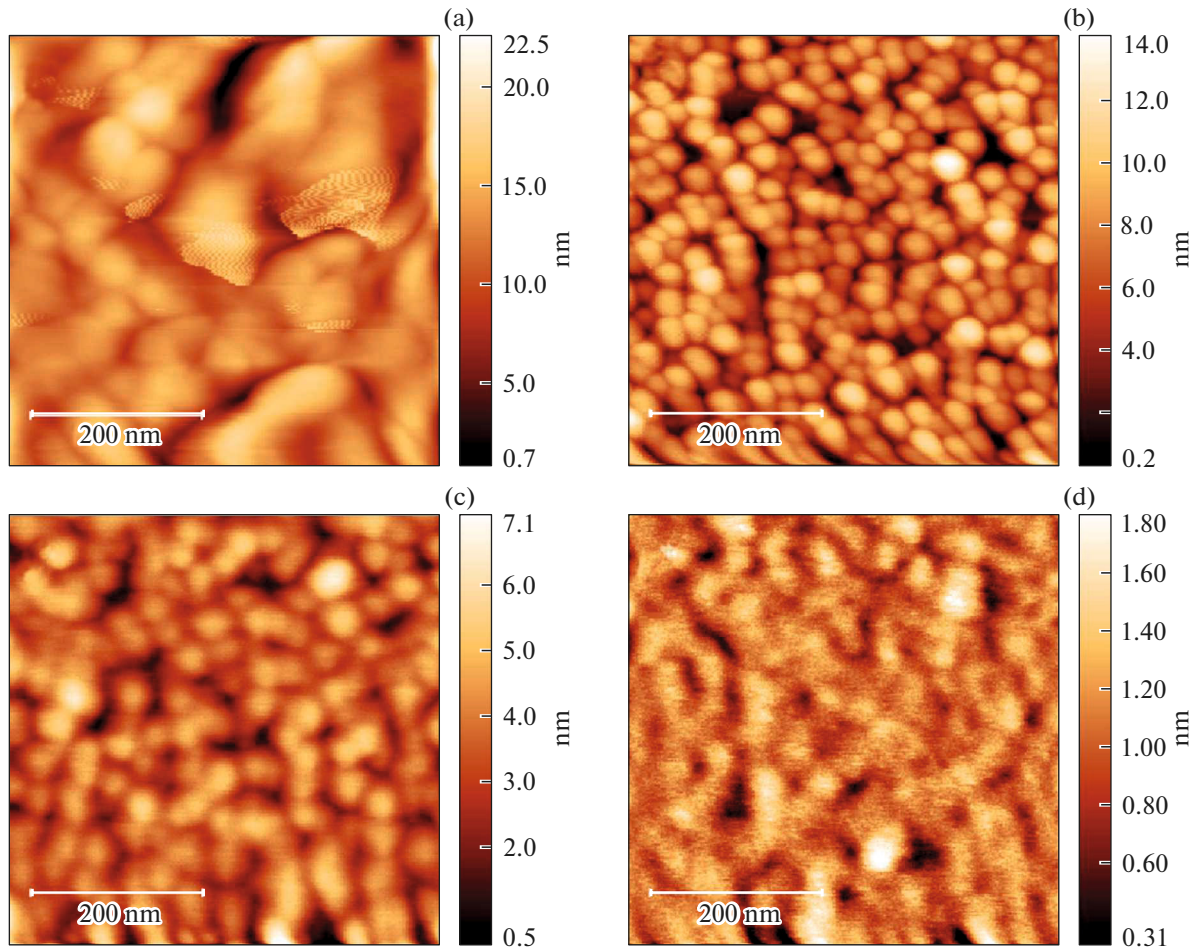
Fig. 4. AFM images of zinc oxide layers obtained by ultrasonic spray pyrolysis with varying application duration, of different thickness: (a)—thickness of the layer of zinc oxide $h \approx 130$ nm; (b)—effective thickness $h_{eff} \approx 19.9$; (c)— 13.3; (d)— 2.6 nm.

discontinuity of the seed layer, since the resistance practically coincides with the resistance of the lower ITO electrode (Fig. 5).

An increase of the thickness of the seed layers to the values of $h_{eff} \approx 13.3$ and ≈ 19.9 nm leads to an increase of resistance. However, the increase of resistance is insignificant, while a further increase of the film thickness by 6−10 times to 130 nm leads to an increase of resistance by almost two orders of magnitude. It can be assumed that the current flow in thin films with $h_{eff} \approx 13.3$ and ≈ 19.9 nm is mainly attributable to grain boundaries, while a more significant increase of resistance in a thick film confirms its continuity.

The high gas sensitivity of adsorption gas sensors is ensured by a high concentration of adsorption centers on the surface of the semiconductor, the characteristic size of the structural element (particle) comparable to the Debye screening length (several nanometers), and a high specific surface area. It is shown from the results of SEM and XPS that the ZnO nanorods obtained in the work have a small diameter, and their surface con-
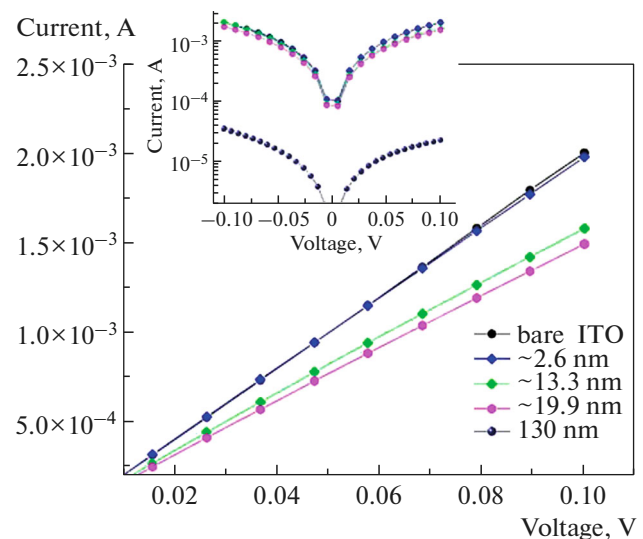

Fig. 5. Volt-ampere characteristics of ZnO seed layers obtained using the lower ITO electrode and the upper electrode based on the eGain liquid probe.
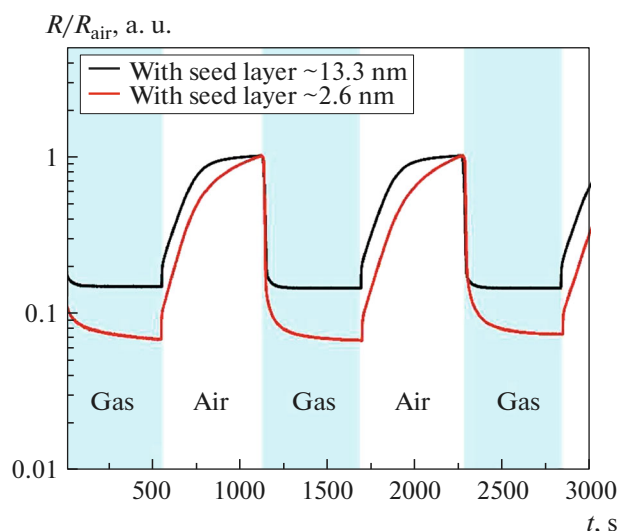
Fig. 6. Normalized change of the resistance of sensor nanostructured coatings made of ZnO nanorods formed on seed layers with an effective thickness of 13.3 and 2.6 nm obtained by ultrasonic spray pyrolysis (for 5 and 1 min, respectively) under cyclic exposure to isopropyl alcohol vapors with a concentration of 1000 ppm. The substrate temperature was about 150°C. Offset voltage—5 V.

Fig. 7. Concentration dependences of the responses of gas-sensitive nanostructured coatings of zinc oxide nanorods formed on seed layers obtained by ultrasonic spray pyrolysis for 5 and 1 min (with an effective thickness of 13.3 and 2.6 nm, respectively).

tains a high concentration of vacancies that serve as adsorption centers. A high specific area of the material is necessary to ensure rapid and efficient diffusion and adsorption of oxygen and then the target gas throughout the entire volume of the material to prevent the flow of current in the material that does not interact with the atmosphere and the target gases-analytes. Therefore, layers with a thickness of ~13.3 and ~2.6 nm were used as seed layers of ZnO to form a sensor coating from nanorods and study their gas sensitivity. The heating temperature of the sensor platforms was chosen to be 150°C, as the minimum operating temperature of modern adsorption resistive gas sensors.

Figure 6 shows the response of sensor coatings made of nanorods using seed layers with an effective thickness of ~13.3 and ~2.6 nm obtained during the spray pyrolysis process of 5 and 1 min, respectively, to isopropyl alcohol vapors. Reducing the duration of application of the seed leads to an increase of the sensory response to isopropyl alcohol vapor.

The response of the sensor coating (R_{air}/R_{gas}) to isopropyl alcohol vapors with a concentration of 1000 ppm increased from ~6 to ~15 with a decrease of the effective thickness of the seed layer from ~13.3 to ~2.6 nm or the duration of application from 5 to 1 min, while an increase of the response is observed over the entire range of isopropyl alcohol concentrations used in measurements (Fig. 7). It should be expected that the resulting sensor coating of ZnO nanorods will have a sufficient response for practical use with a further decrease of the concentrations of analyte gases to the values of ppm units.
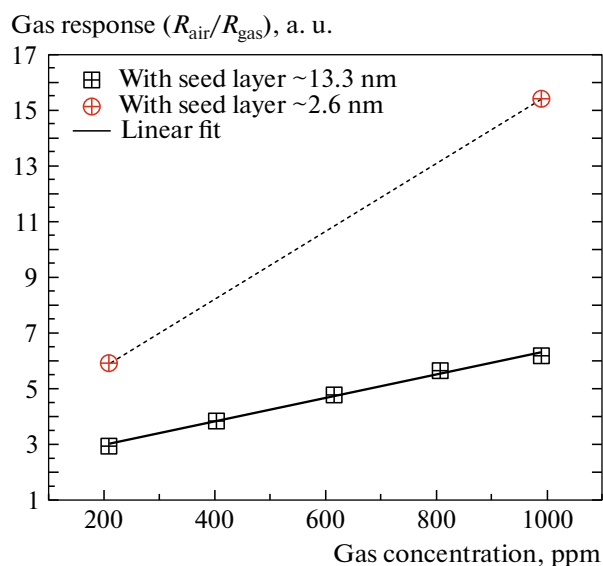
The surface of the ceramic substrate with counter-pin electrodes is protruding grains (Fig. 8), which determine the morphology of the coating in the form of arrays of ZnO nanorods in contact with each other (Figs. 1, 8b). The results of the gas sensitivity study show that an increase of the thickness of the seed layer leads to a decrease of the gas analytical response. This indicates the flow of current not only through the nanorods, where the resistance is modulated by adsorption, but also the seed layer, access to which the adsorbed gas molecules are limited.

Thus, the current flowing in the sensor coating on a ceramic substrate can be divided into current through the nanorods (I_1) and current (I_2) through the seed layer (Fig. 8b). Current measurements through the seed layer using an upper liquid probe indicate the
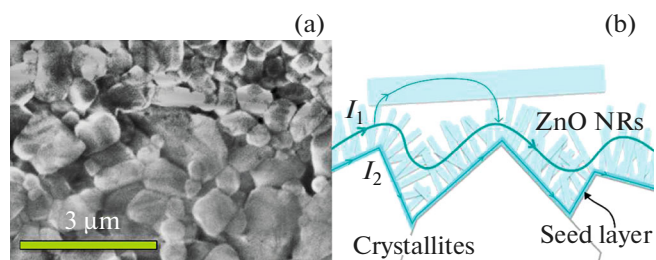

Fig. 8. (a) SEM image of the surface of the ceramic substrate; (b) schematic representation of the ZnO nanorods on the grains of the ceramic substrate and possible paths of current flow through larger nanorods formed in the volume of the solution.

discontinuous nature of the ZnO seed layer at an effective thickness of 2.6 nm. The use of crystallites of the seed layer separated from each other limits the influence of the component I_2 on the gas-analytical response. As shown in Fig. 8b, the current can also flow through nanorods of the second type formed in the volume of the solution, the depleted area of which is insignificant when oxygen ions are adsorbed compared to the diameter of the rods. Nevertheless, these nanorods bypass only the areas between the nanorods coating sites, without affecting the overall nature of the gas-analytical response. This is confirmed by measurements of the gas sensitivity of coatings.

CONCLUSIONS

The low-temperature synthesis technique presented in this paper provides the production of zinc oxide nanorods with a small diameter to achieve a high gas-analytical response. The obtained ZnO nanorods with subsequent annealing in an air atmosphere at a temperature of 500°C demonstrate a high concentration of oxygen vacancies in the near-surface region of the nanorods and a high concentration of adsorbed hydroxyl groups.

It is shown that the reduction of the duration of application of ZnO seed layer by ultrasonic spray pyrolysis to obtain local centers of subsequent growth of nanorods results in an increase of the gas-analytical response of the sensor coating, while the nanorods formed in the volume of the solution do not affect the response. The use of a ceramic substrate with protruding grains provides additional current flow paths due to intersections between the ZnO nanorods.

An additional method is proposed for controlling the seed layers by resistance using a liquid probe based on indium-gallium melt without the need to apply upper contacts.

The short formation time of seed centers by the method of ultrasonic spray pyrolysis, which does not require vacuum, and the simplicity of the equipment of the low-temperature hydrothermal method ensure the suitability of the presented technique for the formation of nanostructured coatings from ZnO nanorods for scaling and mass production of sensor coatings.

CONFLICT OF INTEREST

The authors declare that they have no conflict of interest.

REFERENCES

1. N. Yamazoe, G. Sakai, K. Shimanoe. Catalysis Surveys from Asia, **7**, 63 (2003).
   https://doi.org/10.1023/A:1023436725457

2. A. M. Andringa, C. Piliego, I. Katsouras, P. W. Blom, D. M. D. Leeuw. Chem. Mater., **26** (1), 773 (2014).
   https://doi.org/10.1021/cm4020628

3. V. A. Moshnikov, S. S. Nalimova, B. I. Seleznev. Semiconductors, **48** (11), 1499 (2014).
   https://doi.org/10.1134/S1063782614110177

4. J. Shin, S. J. Choi, I. Lee, D. Y. Youn, C. O. Park, J. H. Lee, H. L. Tuller, I. D. Kim. Advanced Functional Mater., **23** (19), 2357 (2013).
   https://doi.org/10.1002/adfm.201202729

5. G. Katwal, M. Paulose, I. A. Rusakova, J. E. Martinez, O. K. Varghese. Nano Lett., **16** (5), 3014 (2016).
   https://doi.org/10.1021/acs.nanolett.5b05280

6. V. V. Sysoev, B. K. Button, K. Wepsiec, S. Dmitriev, A. Kolmakov. Nano Lett., **6** (8), 1584 (2006).
   https://doi.org/10.1021/nl060185t

7. V. V. Sysoev, J. Goschnick, T. Schneider, E. Strelcov, A. Kolmakov. Nano Lett., **7** (10), 3182 (2007).
   https://doi.org/10.1021/nl071815+

8. A. Bobkov, A. Varezhnikov, I. Plugin, F. S. Fedorov, V. Trouillet, U. Geckle, M. Sommer, V. Goffman, V. Moshnikov, V. Sysoev. Sensors, **19** (19), 4265 (2019).
   https://doi.org/10.3390/s19194265

9. Y. Lin, K. Kan, W. Song, G. Zhang, L. Dang, Y. Xie, P. Shen, L. Li, K. Shi. J. Alloys Compounds, **639**, (2015).
   https://doi.org/10.1016/j.jallcom.2015.03.139

10. S. W. Fan, A. K. Srivastava, V. P. Dravid. Appl. Phys. Lett. **95**, 142106 (2009).
    https://doi.org/10.1063/1.3243458

11. Q. Geng, Z. He, X. Chen, W. Dai, X. Wang. Sensors and Actuators B: Chemical, **188**, 293 (2013).
    https://doi.org/10.1016/j.snb.2013.07.001

12. L. Han, D. Wang, Y. Lu, T. Jiang, B. Liu, Y. Lin. J. Phys. Chem. C, **115** (46), 22939 (2011).
    https://doi.org/10.1021/jp206352u

13. A. S. Chizhov, M. N. Rumyantseva, R. B. Vasiliev, D. G. Filatova, K. A. Drozdov, I. V. Krylov, A. V. Marchevsky, O. M. Karakulina, A. M. Abakumov, A. M. Gaskov. Thin Solid Films, **618**, 253 (2016).
    https://doi.org/10.1016/j.tsf.2016.09.029

14. E. Comini, C. Baratto, G. Faglia, M. Ferroni, A. Vomiero, G. Sberveglieri. Progress in Mater. Sci., **54** (1), 1 (2009).
    https://doi.org/10.1016/j.pmatsci.2008.06.003

15. S. Wang, Z. X. Lin, W. H. Wang, C. L. Kuo, K. C. Hwang, C. C. Hong. Sensors and Actuators B: Chemical, **194**, 1 (2014).
    https://doi.org/10.1016/j.snb.2013.12.042

16. J. D. Prades, R. Jiménez-Dıaz, F. Hernandez-Ramirez, S. Barth, A. Cirera, A. Romano-Rodriguez, S. Mathur, J. R. Morante. Sensors and Actuators B: Chemical, **140** (2), 337 (2009).
https://doi.org/10.1016/j.snb.2009.04.070

17. M. Procek, T. Pustelny, A. Stolarczyk. Nanomaterials, **6** (12), 227 (2016).
https://doi.org/10.3390/nano6120227

18. Y. Sahin, S. Öztürk, N. Kılınç, A. Kösemen, M. Erkovan, Z. Z. Öztürk. Appl. Surf. Sci., **303**, 90 (2014).
https://doi.org/10.1016/j.apsusc.2014.02.083

19. L. Peng, J. Zhai, D. Wang, Y. Zhang, P. Wang, Q. Zhao, T. Xie. Sens. Actuator B, **148**, 66 (2010).
https://doi.org/10.1016/j.snb.2010.04.045

20. A. A. Ryabko, S. S. Nalimova, D. S. Mazing, O. A. Korepanov, A. M. Guketlov, O. A. Aleksandrova, A. I. Maximov, V. A. Moshnikov, Z. V. Shomakhov, A. N. Aleshin. Tech. Phys., **92** (6) 717 (2022).
https://doi.org/10.21883/TP.2022.06.54418.15-22

21. J. Guo, J. Zhang, M. Zhu, D. Ju, H. Xu, B. Cao. Sensors and Actuators B: Chemical, **199**, 339 (2014).
https://doi.org/10.1016/j.snb.2014.04.010

22. M.-W. Ahn, K.-S. Park, J.-H. Heo, J.-G. Park, D.-W. Kim, K. J. Choi, J.-H. Lee, S.-H. Hong. Appl. Phys. Lett., **93**, 263103 (2008).
https://doi.org/10.1063/1.3046726

23. A. Ejsmont, J. Goscianska. Materials, **16** (4), 1641 (2023).
https://doi.org/10.3390/ma16041641

24. S. Barauh, J. Dutta. Sci. Technol. Adv. Mater., **10**, 013001 (2009).
https://doi.org/10.1088/1468-6996/10/1/013001

25. S. Xu, Z. L. Wang. Nano Research, **4**, 1013 (2011).
https://doi.org/10.1007/s12274-011-0160-7

26. S. F. Wang, T. Y. Tseng, Y. R. Wang, C. Y. Wang, H. C. Lu, W. L. Shih. Intern. J. Appl. Ceramic Technol., **5** (5), 419 (2008).
https://doi.org/10.1111/j.1744-7402.2008.02242.x

27. A. A. Ryabko, A. I. Maksimov, V. A. Moshnikov. Vestnik NovGU, **6** (104), 32 (2017).
https://doi.org/10.34680/2076-8052.2019.4(116).40-43

28. S. A. Kadinskaya, V. M. Kondratev, I. K. Kindyushov, O. Y. Koval, D. I. Yakubovsky, A. Kusnetsov, A. I. Lihachev, A. V. Nashchekin, I. K. Akopyan, A. Y. Serov, M. E. Labzovskaya, S. V. Mikushev, B. V. Novikov, I. V. Shtrom, A. D. Bolshakov. Nanomaterials, **13** (1), 58 (2023).
https://doi.org/10.3390/nano13010058

29. H. E. Unalan, P. Hiralal, N. Rupesinghe, S. Dalal, W. Milne, G. Amaratunga. Nanotechnology, **19**, 255608 (2008).
https://doi.org/10.1088/0957-4484/19/25/255608

30. C. Chevalier-César, M. Capochichi-Gnambodoe, Y. Leprince-Wang. Appl. Phys. A, **115**, 953 (2014).
https://doi.org/10.1007/s00339-013-7908-8

31. X. M. Sun, X. Chen, Z. X. Deng, Y. D. Li. Mater. Chem. Phys., **78** (1), 99 (2003).
https://doi.org/10.1016/S0254-0584(02)00310-3

32. N. Permiakov, E. Maraeva, A. Bobkov, R. Mbwahnche, V. Moshnikov. Technologies, **11** (1), 26 (2023).
https://doi.org/10.3390/technologies11010026

33. A. A. Ryabko, A. A. Bobkov, S. S. Nalimova, A. I. Maksimov, V. S. Levitskii, V. A. Moshnikov, E. I. Terukov. Tech. Phys., **67** (5), 644 (2022).
https://doi.org/10.21883/TP.2022.05.53683.314-21

34. S. Iaiche, A. Djelloul. J. Spectrosc., 2015, 836859 (2015).
https://doi.org/10.1155/2015/836859

35. I. A. Pronin, I. A. Averin, A. A. Karmanov, N. D. Yakushova, A. S. Komolov, E. F. Lazneva, M. M. Sychev, V. A. Moshnikov, G. Korotcenkov. Nanomaterials, **12**, 1924 (2022).
https://doi.org/10.3390/nano12111924

36. M. Kwoka, A. Kulis-Kapuscinska, D. Zappa, E. Comini, J. Szuber. Nanotechnology, **31** (46), 465705 (2020).
https://doi.org/10.1088/1361-6528/ab8dec

37. R. Al-Gaashani, S. Radiman, A. R. Daud, N. Tabet, Y. Al-Douri. Ceram. Int., **39**, 2283 (2013).
https://doi.org/10.1016/j.ceramint.2012.08.075

38. E. Grånäs, M. Busch, B. Arndt, M. Creutzburg, G. D. L. Semione, J. Gustafson, A. Schaefer, V. Vonk, H. Grönbeck, A. Stierle. Commun. Chem., **4**, 7 (2021).
https://doi.org/10.1038/s42004-020-00442-6

39. R. Heinhold, M. W. Allen. J. Mater. Res., **27** (17), 2214 (2012).
https://doi.org/10.1557/jmr.2012.181

40. X. Zhang, J. Qin, Y. Xue, P. Yu, B. Zhang, L. Wang, R. Liu. Scientific Reports, **4** (1), 1 (2014).
https://doi.org/10.1038/srep04596

Translated by Ego Translating